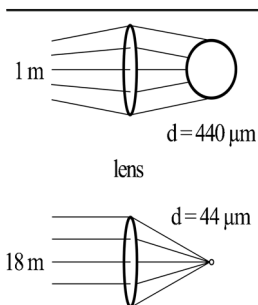


A Simple Method for Improving the Spatial Resolution in Infrared Laser Ablation Mass Spectrometry Imaging

Juha-Pekka Hieta, Anu Vaikkinen, Samuli Auno, Heikki Rääkkönen, Markus Haapala, Gianmario Scotti, Jaakko Kopra, Petteri Piepponen, Tiina J. Kauppila

Faculty of Pharmacy, University of Helsinki, P.O. Box 5600014, Helsinki, Finland



Abstract. In mass spectrometry imaging of tissues, the size of structures that can be distinguished is determined by the spatial resolution of the imaging technique. Here, the spatial resolution of IR laser ablation is markedly improved by increasing the distance between the laser and the focusing lens. As the distance between the laser and the lens is increased from 1 to 18 m, the ablation spot size decreases from 440 to 44 μm . This way, only the collimated center of the divergent laser beam is directed on the focusing lens, which results in better focusing of the beam. Part of the laser energy is lost at longer distance, but this is compensated by focusing of the radiation to a smaller area on the sample surface. The long distance can also be achieved by a set of mirrors, between which the radiation travels before it is directed to the focusing

lens and the sample. This method for improving the spatial resolution can be utilized in mass spectrometry imaging of tissues by techniques that utilize IR laser ablation, such as laser ablation electrospray ionization, laser ablation atmospheric pressure photoionization, and matrix-assisted laser desorption electrospray ionization.

Keywords: Mass spectrometry imaging, IR laser ablation, Tissue imaging, Spatial resolution, Ambient mass spectrometry, Laser ablation electrospray ionization, Laser ablation atmospheric pressure photoionization, Matrix-assisted laser desorption electrospray ionization, Metastable-induced chemical ionization, Laser focusing

Received: 30 September 2016/Revised: 25 November 2016/Accepted: 10 December 2016/Published Online: 11 January 2017

Introduction

Infrared (IR) laser ablation is an efficient means for ablating particulates from the surfaces of water-containing samples, such as plant and animal tissues [1]. IR laser ablation is utilized in several ambient mass spectrometry techniques, such as laser ablation electrospray ionization (LAESI) [2], matrix-assisted laser desorption electrospray ionization (MALDESI) [3], infrared laser ablation metastable-induced chemical ionization (IR-LAMICI) [4], and laser ablation atmospheric pressure photoionization (LAAPPI) [5]. A major advantage of IR laser ablation is that in contrast to UV laser ablation, which is used in, e.g., matrix-assisted laser desorption/ionization (MALDI), IR laser ablation does not require the addition of a light-absorbing matrix. Instead, the radiation of the IR laser at 2.94 μm is

efficiently absorbed by water molecules, which are naturally abundant in tissue samples. Absorption of the IR laser radiation by water leads to explosive evaporation of water and ablation of the target. Ionization at this step is inefficient and, therefore, the neutral analytes within the plume are typically ionized by varying post-ionization methods, such as electrospray ionization (e.g., LAESI and MALDESI), metastable-induced chemical ionization (e.g., IR-LAMICI), or photoionization (e.g., LAAPPI).

Owing to the efficient ablation of tissues, IR laser ablation has been extensively utilized in MS imaging of plant and animal tissues [6–14]. In MS imaging, the size of the structures that can be distinguished is dependent on the spatial resolution of the desorption/ablation technique in question (i.e., in case of laser ablation, the size of the ablated spot). Typically, spot sizes that have been reported with IR laser ablation are in the range of 220–400 μm [2, 4, 9, 15, 16]. Smaller spot size has been achieved by delivering the mid-IR laser pulses through an etched tip of a glass fiber, which is placed in close proximity of the sample [17]. The tip confines the laser beam to the diameter of the tip, and roughly 30–40 μm ablation spot

Electronic supplementary material The online version of this article (doi:10.1007/s13361-016-1578-7) contains supplementary material, which is available to authorized users.

Correspondence to: Tiina J. Kauppila; e-mail: tiina.kauppila@helsinki.fi

diameters have been achieved by this method in LAESI. This, however, requires very careful positioning of the fiber tip and exposes it to ablated sample material. On the other hand, this setup may decrease sensitivity due to partial blockage of the ejected plume by the fiber. In atmospheric pressure-infrared laser desorption/ionization, 30 μm diameter spots have been reported with a complicated optical setup including a coaxially lined IR objective lens [18]. Spot sizes of 10–20 μm have been achieved in LAESI using transmission geometry and an objective lens with a high numerical aperture [19]. This approach has been used for analysis of adherent mammalian cells *in situ*. Another approach to reach better resolution without the need for matrix is to use a shorter pulse length than in typically applied nanosecond lasers. Lateral resolution of 100 μm has been achieved using picosecond IR laser pulses [20]. Such lasers, however, are very expensive and available to few researchers. Furthermore, using a 25 μm pinhole to filter the beam of a UV laser has been reported to lead to 5 μm laser spot size in MALDI imaging [21], and would possibly function also with an IR laser.

In this contribution, we present an easy and inexpensive method for improving the ablation spot size in IR laser ablation to at least 44 μm by simply increasing the length of the laser beam path. This method will be useful for researchers working with different IR-laser based ambient mass spectrometry imaging methods.

Experimental

All animal experiments were approved by the National Animal Experiment Board of Finland (License number ESAVI/11198/04.10.07/2014). Mice from a triple mixed genetic background (129Ola/ICR/C57Bl6) were anesthetized with an overdose of sodium pentobarbital (100 mg/kg, *i.p.*). Anesthetized animals were transcardially perfused with warm phosphate buffered saline (PBS) for 4 min followed by 4% paraformaldehyde (PFA) in 0.1 M phosphate buffer, pH 7.4, for at least 5 min. The brains were removed and postfixed in the same PFA solution overnight in room temperature and then stored in phosphate buffer containing 20% sucrose at 4 °C. Coronal striatal sections were cut into 30 μm thickness with a cryomicrotome (Leica CM 3050; Leica Microsystems Nussloch GmbH, Nussloch, Germany). The sections were saved in a serial order at –20 °C in cryoprotectant buffer containing glycerol and ethylene glycol. Before the MS analysis, the sections were flushed with Milli-Q water (Merck Millipore, Molsheim, France).

For laser energy and spot size measurements, a mid-IR laser beam was delivered on the sample surface using a gold-coated mirror (PF10-03-M01; Thorlabs, Newton, MA, USA) and focused by an anti-reflection coated 100 mm focal length plano-convex CaF_2 lens (LA5817-E, Thorlabs). The mirror and the lens both had a diameter of 1 inch. The laser was an IR Opolette HE 2940 fixed wavelength and flashlamp pumped Nd:YAG laser operating at 2.94 μm wavelength and 20 Hz repetition rate (Opotek, Carlsbad, CA, USA). The laser energy

was set to 6 mJ/pulse. The ablation holes were created at 1–18 m laser aperture to lens distances, the beam was focused with the lens, and the spots were measured using a Leica DMC2900 camera module attached to a Leica DM6000 B research microscope with 2.5 \times –5 \times objectives (Wezlar, Germany). The reported ablation spot diameters are the averages of maximum and minimum Feret diameters of the spots created with a specific distance. The laser energy was measured using a thermal power sensor (Thorlabs S310C, $d = 20$ mm), which was connected to an energy meter (Thorlabs PM100D). The sensor was first attached to the laser output aperture for measurement of the maximum output, after which the laser energy was measured at distances of 1–18 m. The measurements were carried out in normal laboratory lighting, and therefore the background energy was always measured first.

The mass spectra for the MS images were collected using a Bruker MicrOTOF mass spectrometer (Bremen, Germany). The commercial ion source of the mass spectrometer was replaced by a self-built LAAPPI source, similar to the one described in literature [5, 6]. The mass spectrometer was equipped with a modified extension capillary. An aluminum shield was attached to the outer part of the extension capillary to direct the drying gas to the sides, away from the ionization area. The drying gas temperature was 250 °C, and the gas was supplied at 5 L/min. The capillary exit and skimmers 1 and 2 voltages were set to 240, 80, and 23 V, respectively. The data acquisition time was set to 1 Hz, and the dwell-time was 35 s. The ablation plume was intercepted by a hot acetone (Sigma-Aldrich, HPLC grade [99.8%], Steinheim, Germany) vapor jet, which was directed toward the inlet of the mass spectrometer. The jet was produced using an all-glass heated nebulizer microchip, described previously in detail [22]. The liquid solvent (acetone) was introduced into the heated nebulizer microchip at 10 $\mu\text{L}/\text{min}$ using an Agilent 1100 capillary LC pump (Waldbronn, Germany), and vaporized with the aid of nitrogen gas flow (100 mL/min) and high temperature (4.0 W heating power producing ~ 350 °C jet temperature at 5 mm of the chip nozzle [23]). The tissue sections were placed on a microscope glass slide mounted on a Peltier cooling stage and positioned in front of the mass spectrometer ~ 3 mm below the inlet orifice. The temperature of the Peltier stage was kept at 5 °C in order to minimize dehydration and to optimize the amount of water for the ablation process. The sample plume and solvent jet were irradiated in the ambient air with 10.0 and 10.6 eV photons produced by a krypton discharge vacuum ultraviolet (VUV) photoionization lamp (PKR 100; Heraeus Noblelight, Cambridge, UK). The tissue sample was rastered by moving the cooled stage in the *xy*-plane using two computer-controlled motorized 100 mm linear translation stages (NRT100/M; Thorlabs). The mass spectra were collected using Compass 1.3 for micrOTOF (Bruker). The *XY* stage and the IR laser were controlled by a self-written MATLAB-based program. Time and stage position data were recorded during the

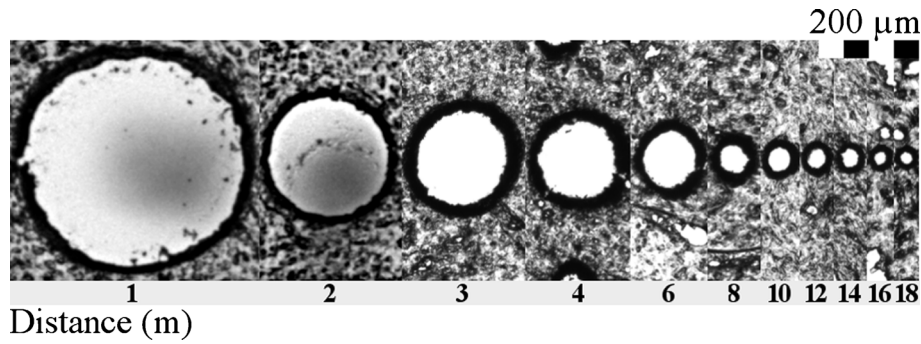


Figure 1. IR laser ablation holes created on a 30 μm thick mouse tissue at 1–18 m distance between the laser aperture and the focusing lens. Note: a Peltier cooling stage was not used in this measurement series

imaging experiment. This information was later used to split the measurement file into pixel files. Each pixel was created by selecting the measurement time interval of the corresponding pixel, and forming an average mass spectrum from the collected spectra. The measurement file was converted to *mz5* file format [24] using ProteoWizard's *msconvert* tool [25] before processing the data with MATLAB. Heatmaps were created with a MATLAB based MSiReader software [26].

Results and Discussion

The spatial resolution of laser ablation was observed to improve significantly by increasing the distance of the laser aperture from the focusing lens. Figure 1 shows the ablation holes caused by 20 IR laser shots (20 Hz) on 30 μm thick mouse brain tissue at distances of 1–18 m between the laser aperture and the focusing lens. While at 1 m distance the average Feret diameter of the spots was 440 μm , at 14 m, an average spot diameter of 55 μm was achieved. We suggest that

this phenomenon is caused by the divergence of photons within the noncollimated, multimodal laser beam. According to the laser manufacturer (OPOTEK), the laser beam has a divergence of 10 mrad in the x-axis and 5 mrad in the y-axis; the beam profile is shown in Supplementary Figure S1 in the Supporting Material. At short distance, the focusing lens collects most of the photons within the laser beam, and thus the aberration is larger since the angles at which the photons arrive to the lens have a wide distribution (Fig. 2). As the distance to the focusing lens increases, only the most collimated center of the laser beam is collected, while the diverted photons are lost. Since the lens now focuses more uniform light, the aberration and the spot size are reduced.

Figure 3 shows the experimentally measured spot diameters, laser energies, and fluencies at 1–18 m laser aperture-focusing lens distances (Supplementary Tables S1–S3 show the measured and calculated values). The spot size decreases first exponentially, but then levels off, probably since most of the diverted photons are already lost at the first meters.

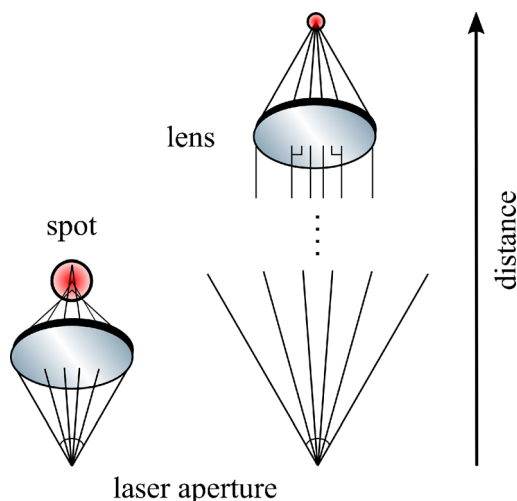


Figure 2. At short distance, photons with different flight paths are efficiently captured by the focusing lens and, as a consequence, the resulting ablation area is large (*left*). At long distance, diverted photons fail to hit the focusing lens, and the photons hit the lens in a similar angle. Thus, the resulting ablation area is very small (*right*)

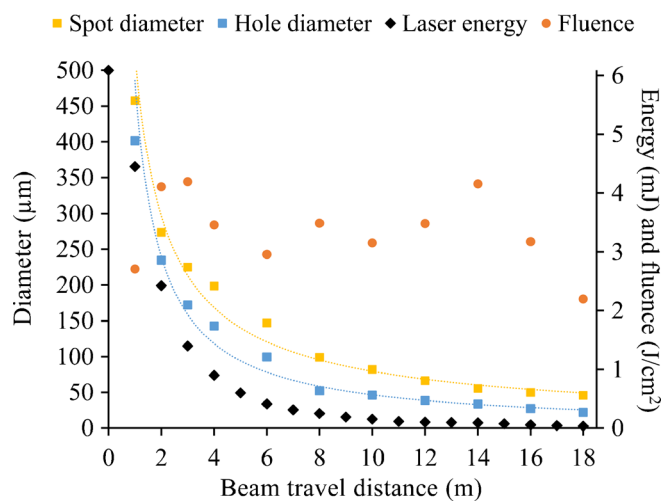


Figure 3. Effect of the distance between the laser aperture and the focusing lens on the average Feret diameters of the ablation spots and holes, the energy reaching the focusing lens, and the fluence on target. (Note: the presented values for laser energy and fluence are based on measurements with 20 mm o.d. thermal power sensor and are thus underestimations of the amount of photons arriving at the lens with 25.4 mm o.d.)

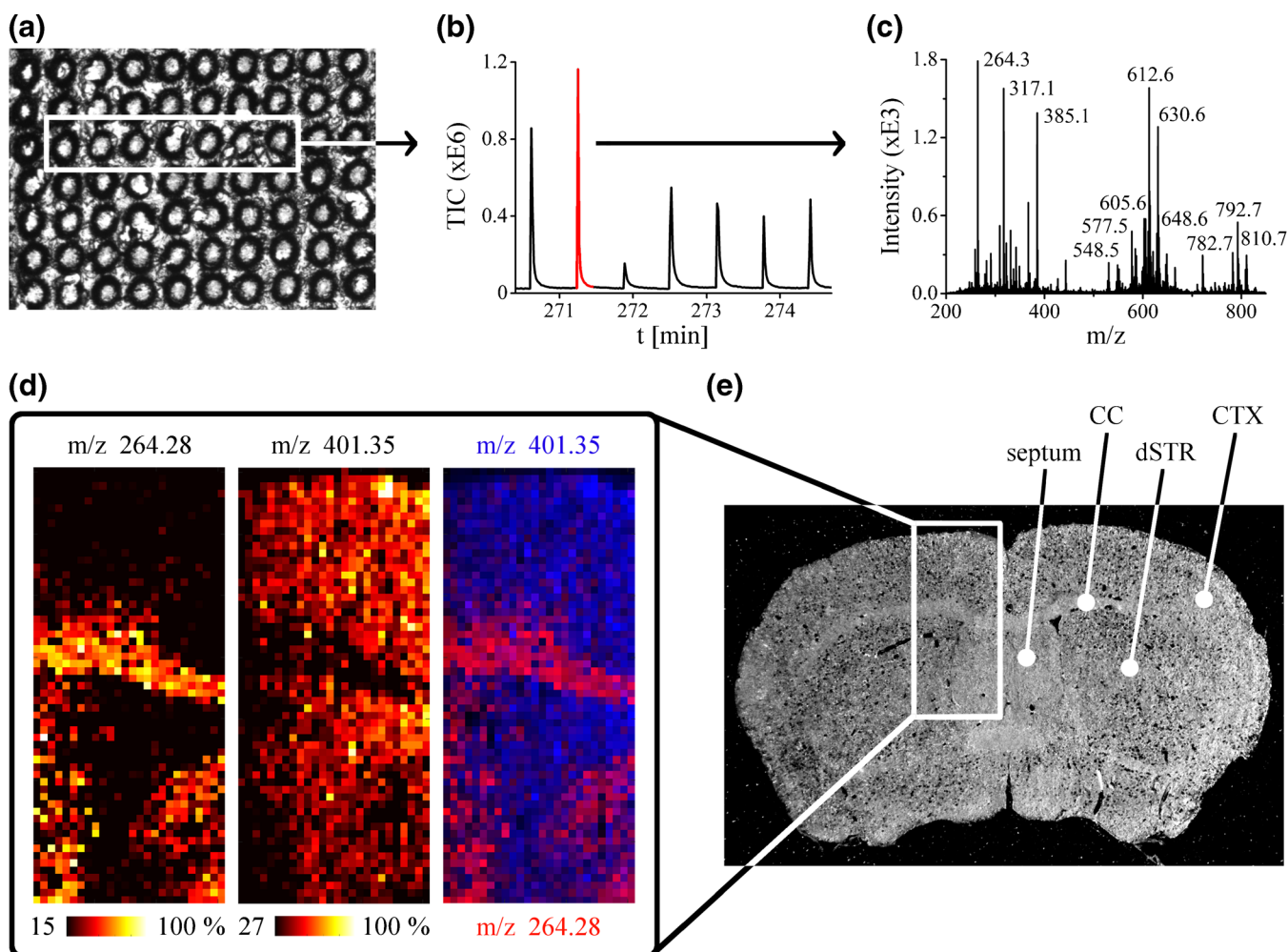


Figure 4. (a) Partial microscope picture of the imaged area showing the spots created with laser ablation using a 60 μm step size. The measured average ablation spot and hole diameters were 55 μm and 30 μm , respectively. (b) Partial total ion chromatogram showing the typical signal intensities achieved from the ablation spot in the imaging experiment with LAAPPI. (c) A single mass spectrum obtained in the MS imaging experiment with LAAPPI. (d) Distributions of ions at $m/z = 264.28$ and $m/z = 401.35$ measured from a 1.56×3.54 mm size area of a 30 μm thick mouse brain tissue with LAAPPI-MS using a 9 m laser beam-focusing lens distance and a Peltier cooling stage. The ion intensities were scaled against the total ion current. (e) Microscopic image showing the rastered tissue area

Supplementary Figure S2 shows the trendlines calculated based on the experimentally defined values for the spot and hole diameters and the laser beam travel distance. A good correlation ($R^2 = 0.98$) between the fitted curve and measured values is observed in both cases.

Decreasing the spot size below ~ 40 μm becomes impractical due to space limitations, although very long optical paths can be achieved with suitably tilted mirrors, between which the laser beam is reflected several times. An example of such a setup (also used in the MS imaging experiment described below) is shown in Supplementary Figure S3. Of course, several reflections reduce the laser energy due to imperfect transmission. However, for a MS imaging experiment, 50 μm spot diameter is usually a practical compromise between the amount of structural information and measurement time, and with the current setup it can be reached with 14 m distance (or less, if a cooling stage is used, see discussion below).

As the distance that the laser beam needs to travel increases, a smaller proportion of photons will finally reach the focusing lens and the sample, and less energy will be available for the ablation process. The plot of laser energy reaching the focusing lens (mJ) follows largely a similar curve as the spot size (Fig. 3), as shown by thermal power sensor measurements. However, since the laser beam can now be focused to a smaller area, the laser fluence (J/cm^2) is in the same order of magnitude with all the distances, and efficient ablation is achieved even at the longest laser distances. Some fluctuations are observed in the laser fluence (Fig. 3). This is partly explained by the uncertainty of the measurement of the irregularly formed spot diameters. Further, as shown in Supplementary Figure S1, the multimodal laser beam contains intensity variations, so-called “hot spots”, and the most intense part of the laser is not in the middle of the beam. As a result, increasing the beam travel distance also changes the intensity profile of the focused beam, which in

turn leads to small intensity and fluence variations across different aperture-focusing lens distances. Moreover, at fixed optical set-up, the produced ablation spots were quite uniform as presented in Fig. 4a, which shows a microscope image of an array of ablated spots on the analyzed tissue area.

To demonstrate the utility of the small ablation spot sizes in MS imaging of a clinical sample, a rectangular area on a coronal mouse brain tissue slice close to the bregma line [27] was imaged using IR laser ablation with 9 m laser beam travel distance resulting in 55 μm spot size, and LAAPPI. Microscopic image of the ablated spots, total ion chromatogram and mass spectrum obtained from the tissue, as well as MS images of two ions are shown in Fig. 4a–e. A slightly smaller spot size with this distance was achieved here than in the experiment shown in Figs. 1 and 3 because here the sample was cooled using a Peltier stage, which is thought to reduce heat propagation in the sample. Beam instability or vibrations were not observed during the measurement, regardless of the long laser beam travel distance (Fig. 4a). As an example, Fig. 4d shows the heatmaps of two ions with highly distinct distributions. The ion at m/z 264.28, which is highly abundant in the corpus callosum (CC), dorsal striatum (dSTR), and septum areas (Fig. 4e), is suggested to be a $\text{C}_{18}\text{H}_{34}\text{N}^+$ fragment of sphingosines. The ion at 401.35, on the other hand, which shows an intense signal from the cortex (CTX) area and around the region of lateral ventricle, is suggested to be oxidized cholesterol ($[\text{M} - \text{H} + \text{O}]^+$), or the protonated molecule of ketocholesterol [5]. Furthermore, very intense signals compared with the background were obtained from the ablated spots, as shown in the total ion chromatogram in Fig. 4b, and therefore it is proposed that the signals of even smaller spots are measurable with the current mass spectrometric setup.

Conclusions

A significant improvement to the spatial resolution in IR laser ablation was achieved by simply increasing the distance between the IR laser and the focusing lens. The setup is easy to reproduce, and it does not require expensive optics or fragile fibers. Even 44 μm spot size was achieved, which is sufficiently small for most biological imaging applications. Even smaller spot sizes are achievable using a cooling stage under the sample, as was shown in the MS imaging experiment of a tissue sample. The introduced technique for improving the spatial resolution can be utilized in, e.g., LAESI, LAAPPI, IR-LAMICI, and MALDESI. Current work in our laboratory is focused on MS imaging by LAAPPI and LAESI with high spatial resolution, and a more detailed description of the imaging experiments with whole tissue heatmaps will be published in upcoming work.

Acknowledgments

Yhtyneet/Medix Laboratories is acknowledged for donation of the Bruker MicroTOF mass spectrometer. Academy of Finland

(projects #275089, #2515752, and #276627) is acknowledged for funding.

References

- Vogel, A., Venugopalan, V.: Mechanisms of pulsed laser ablation of biological tissues. *Chem. Rev.* **103**, 577–644 (2003)
- Nemes, P., Vertes, A.: Laser ablation electrospray ionization for atmospheric pressure, in vivo, and imaging mass spectrometry. *Anal. Chem.* **79**, 8098–8106 (2007)
- Sampson, J.S., Hawkridge, A.M., Muddiman, D.C.: Generation and detection of multiply-charged peptides and proteins by matrix-assisted laser desorption electrospray ionization (MALDESI) fourier transform ion cyclotron resonance mass spectrometry. *J. Am. Soc. Mass Spectrom.* **17**, 1712–1716 (2006)
- Galhena, A.S., Harris, G.A., Nyadong, L., Murray, K.K., Fernández, F.M.: Small molecule ambient mass spectrometry imaging by infrared laser ablation metastable-induced chemical ionization. *Anal. Chem.* **82**, 2178–2181 (2010)
- Vaikkinen, A., Shrestha, B., Kauppila, T.J., Vertes, A., Kostianen, R.: Infrared laser ablation atmospheric pressure photoionization mass spectrometry. *Anal. Chem.* **84**, 1630–1636 (2012)
- Vaikkinen, A., Shrestha, B., Koivisto, J., Kostianen, R., Vertes, A., Kauppila, T.J.: Laser ablation atmospheric pressure photoionization mass spectrometry imaging of phytochemicals from sage leaves. *Rapid Commun. Mass Spectrom.* **28**, 2490–2496 (2014)
- Nemes, P., Barton, A.A., Vertes, A.: Three-dimensional imaging of metabolites in tissues under ambient conditions by laser ablation electrospray ionization mass spectrometry. *Anal. Chem.* **81**, 6668–6675 (2009)
- Vaikkinen, A., Shrestha, B., Nazarian, J., Kostianen, R., Vertes, A., Kauppila, T.J.: Simultaneous detection of nonpolar and polar compounds by heat-assisted laser ablation electrospray ionization mass spectrometry. *Anal. Chem.* **85**, 177–184 (2013)
- Nemes, P., Barton, A.A., Li, Y., Vertes, A.: Ambient molecular imaging and depth profiling of live tissue by infrared laser ablation electrospray ionization mass spectrometry. *Anal. Chem.* **80**, 4575–4582 (2008)
- Nemes, P., Woods, A.S., Vertes, A.: Simultaneous imaging of small metabolites and lipids in rat brain tissues at atmospheric pressure by laser ablation electrospray ionization mass spectrometry. *Anal. Chem.* **82**, 982–988 (2010)
- Li, H., Smith, B.K., Mark, L., Nemes, P., Nazarian, J., Vertes, A.: Ambient molecular imaging by laser ablation electrospray ionization mass spectrometry with ion mobility separation. *Int. J. Mass Spectrom.* **377**, 681–689 (2015)
- Loziuk, P., Meier, F., Johnson, C., Ghashghaei, H.T., Muddiman, D.C.: TransOmic analysis of forebrain sections in Sp2 conditional knockout embryonic mice using IR-MALDESI imaging of lipids and LC-MS/MS label-free proteomics. *Anal. Bioanal. Chem.* **408**, 3453–3474 (2016)
- Bokhart, M.T., Rosen, E., Thompson, C., Sykes, C., Kashuba, A.D.M., Muddiman, D.C.: Quantitative mass spectrometry imaging of emtricitabine in cervical tissue model using infrared matrix-assisted laser desorption electrospray ionization. *Anal. Bioanal. Chem.* **407**, 2073–2084 (2015)
- Barry, J.A., Groseclose, M.R., Robichaud, G., Castellino, S., Muddiman, D.C.: Assessing drug and metabolite detection in liver tissue by UV-MALDI and IR-MALDESI mass spectrometry imaging coupled to FT-ICR MS. *Int. J. Mass Spectrom.* **377**, 448–455 (2015)
- Laiko, V.V., Taranenko, N.I., Berkout, V.D., Yakshin, M.A., Prasad, C.R., Lee, H.S., Doroshenko, V.M.: Desorption/ionization of biomolecules from aqueous solutions at atmospheric pressure using an infrared laser at 3 μm . *J. Am. Soc. Mass Spectrom.* **13**, 354–361 (2002)
- Sampson, J.S., Murray, K.K., Muddiman, D.C.: Intact and top-down characterization of biomolecules and direct analysis using infrared matrix-assisted laser desorption electrospray ionization coupled to FT-ICR mass spectrometry. *J. Am. Soc. Mass Spectrom.* **20**, 667–673 (2008)
- Shrestha, B., Vertes, A.: In situ metabolic profiling of single cells by laser ablation electrospray ionization mass spectrometry. *Anal. Chem.* **81**, 8265–8271 (2009)
- Römpp, A., Schäfer, K.C., Guenther, S., Wang, Z., Köstler, M., Leisner, A., Paschke, C., Schramm, T., Spengler, B.: High-resolution atmospheric

- pressure infrared laser desorption/ionization mass spectrometry imaging of biological tissue. *Anal. Bioanal. Chem.* **405**, 6959–6968 (2013)
19. Jacobson, R.S., Thurston, R.L., Shrestha, B., Vertes, A.: In situ analysis of small populations of adherent mammalian cells using laser ablation electrospray ionization mass spectrometry in transmission geometry. *Anal. Chem.* **87**, 12130–12136 (2015)
 20. Zou, J., Talbot, F., Tata, A., Ermini, L., Franjic, K., Ventura, M., Zheng, J., Ginsberg, H., Post, M., Ifa, D.R., Jaffray, D., Miller, R.J.D., Zarrine-Afsar, A.: Ambient mass spectrometry imaging with picosecond infrared laser ablation electrospray ionization (PIR-LAESI). *Anal. Chem.* **87**, 12071–12079 (2015)
 21. Zavalin, A., Yang, J., Caprioli, R.: Laser beam filtration for high spatial resolution MALDI imaging mass spectrometry. *J. Am. Soc. Mass Spectrom.* **24**, 1153–1156 (2013)
 22. Saarela, V., Haapala, M., Kostiainen, R., Kotiaho, T., Franssila, S.: Glass microfabricated nebulizer chip for mass spectrometry. *Lab Chip* **7**, 644–646 (2007)
 23. Saarela, V., Haapala, M., Kostiainen, R., Kotiaho, T., Franssila, S.: Microfluidic heated gas jet shape analysis by temperature scanning. *J. Micromech. Microeng.* **19**, 055001 (2009)
 24. Wilhelm, M., Kirchner, M., Steen, J.A.J., Steen, H.: mz5: Space- and time-efficient storage of mass spectrometry data sets. *Mol. Cell. Proteomics* **11**, O111.011379 (2012)
 25. Chambers, M.C., Maclean, B., Burke, R., Amodei, D., Ruderman, D.L., Neumann, S., Gatto, L., Fischer, B., Pratt, B., Egertson, J., Hoff, K., Kessner, D., Tasman, N., Shulman, N., Frewen, B., Baker, T.A., Brusniak, M.-Y., Paulse, C., Creasy, D., Flashner, L., Kani, K., Moulding, C., Seymour, S.L., Nuwaysir, L.M., Lefebvre, B., Kuhlmann, F., Roark, J., Rainer, P., Detlev, S., Hemenway, T., Huhmer, A., Langridge, J., Connolly, B., Chadick, T., Holly, K., Eckels, J., Deutsch, E.W., Moritz, R.L., Katz, J.E., Agus, D.B., MacCoss, M., Tabb, D.L., Mallick, P.: A cross-platform toolkit for mass spectrometry and proteomics. *Nat. Biotech.* **30**, 918–920 (2012)
 26. Robichaud, G., Garrard, K.P., Barry, J.A., Muddiman, D.C.: MSiReader: an open-source interface to view and analyze high resolving power MS imaging files on matlab platform. *J. Am. Soc. Mass Spectrom.* **24**, 718–721 (2013)
 27. Franklin, K.B.J., Paxinos, G.: *The mouse brain in stereotaxic coordinates*. Academic Press, San Diego (1997)